Evaporation-induced flow in an inviscid liquid line at any contact angle

A. J. Petsi and V. N. Burganos*
Institute of Chemical Engineering and High Temperature Chemical Processes, Foundation for Research and Technology, Hellas, Greece and Department of Chemical Engineering, University of Patras, 26504, Patras, Greece
(Received 22 November 2005; published 27 April 2006)

The problem of potential flow inside an evaporating liquid line, shaped as an infinitely long cylindrical segment lying on a flat surface, is considered and an analytical solution is obtained for *any* contact angle in $(0,\pi)$. In this way, microflow details inside linear liquid bodies evaporating on hydrophilic, hydrophobic, and strongly hydrophobic substrates can now be obtained. The mathematical formulation employs the velocity potential and stream function formulations in bipolar coordinates and the solution is obtained using the technique of Fourier transform. Both pinned and depinned contact lines are considered. The solution is applicable to any evaporation mechanism but for illustration purposes numerical results are presented here for the particular case of kinetically controlled evaporation. For hydrophilic substrates, the flow inside the evaporating liquid line is directed towards the edges for pinned contact lines, thus, promoting a coffee stain effect. The opposite flow direction is observed for depinned contact lines. However, for strongly hydrophobic substrates, flow is directed outwards for both pinned and depinned contact lines, but owing to its low magnitude compared to that on hydrophilic substrates, a craterlike colloidal deposit should be expected rather than a ringlike deposit, in agreement with experimental observations.

DOI: 10.1103/PhysRevE.73.041201 PACS number(s): 47.55.D−

I. INTRODUCTION

There is a rapidly growing technological and scientific interest in hydrodynamics and mass transport phenomena during droplet evaporation on solid or liquid substrates. Recent technological drives include ink-jet printing and patterning [1], DNA and protein microarray technologies [2,3], fabrication of light emitting diodes [4] and thin film transistors [1,5,6], development of microvessels and microlenses in polymers [7], and desiccated state preservation of mammalian cells [8]. The evaporation of liquid segments with cylindrical geometry, in particular, is encountered in numerous applications, including ink-jet printing and direct write technologies for rapid prototyping and flexible microelectronics, product marking and coding, fine substrate patterning for diverse applications [4–6], etc. It is widely recognized that the evaporation-induced microflow in the interior of the liquid body controls the dynamics of the suspended matter during the evaporation process. Typical examples include the morphology of the particle deposition in the case of evaporating colloid suspensions (e.g., for fine metal wire production [6]) and the alignment of entangled molecules under the action of shear stress (e.g., for optical gene mapping [9]).

For modeling purposes, the usually short characteristic time of spreading compared to that of evaporation justifies the assumption of a quasistatic evaporation stage, which, in turn, allows the consideration of spherical or cylindrical cap geometries due to the action of the surface tension. The cylindrical shape describes satisfactorily the surface of the liquid body that forms from the sequential ejection of identical spherical droplets, aligned along a specific direction. The relatively short spreading time compared to the evaporation time, mentioned above, also justifies the assumption that the coalescence of these droplets into a fine liquid line is practically completed prior to the initiation of the major stage of the evaporation process [10].

A quick measure of the inward or outward flow trend during evaporation is provided by the vertically-averaged velocity of the liquid, which is calculated in a straightforward manner from a mass balance across a differential liquid column [10,11]. The particular characteristics of the evaporation process enter this simple calculation through the value of the local evaporation rate, which, in turn, is a function of the evaporation mechanism and the rate of the liquid column decrease during evaporation. The latter depends on the local evaporation rate also but, in addition, is strongly affected by the mobility of the contact lines. More specifically, the contact lines may remain pinned or recede during evaporation. The former case has been repeatedly verified experimentally for droplets made up of colloidal suspensions, at least at the initial stages of the evaporation process. Pure solvents, on the other hand, usually evaporate at constant contact angle combined with receding contact lines [10,12–18]. However, the two modes have also been observed to combine in several cases and succeed one another along the progress of evaporation. In general, the behavior of the contact lines is a strong function of several factors, including the rheological properties of the evaporating liquid, the nature and morphology of the substrate, the rate of the evaporation process, and the evaporation mechanism itself.

Although useful in many respects, the aforementioned mass balance can only give a rough estimate of the microflow inside the evaporating liquid. For reasons already explained above, the determination of the local flow field and shear stress in the interior of the liquid body is strongly desired as a function of the evaporation rate, the contact angle, and the mode of contact line motion along the course

*Author to whom correspondence should be addressed. Electronic mail: vbur@iceht.forth.gr

of the evaporation process. To this end, an analytical solution was recently produced in [19], assuming a hemispherical droplet and potential flow conditions inside the droplet. Thanks to the use of a contact angle equal to $\pi/2$, the evaporation flux is uniform on the surface of the droplet in both the diffusion and the kinetic regime. Lubrication solutions for the flow field have also appeared in the literature [9,20], but their validity is expected to be limited to thin droplets only. The accuracy of the lubrication approach in the evaporation of spherical droplets was recently investigated through a comparison with a numerical solution [21].

In a previous publication [22], the authors developed an analytical solution for potential flow inside an evaporating liquid body, shaped as an infinitely long cylindrical segment lying on a flat substrate with a contact angle of $\pi/2$. The solution was obtained using the stream function and velocity potential formulations, assuming pinned contact lines and uniform evaporation flux on the hemicylindrical surface.

In the present work, the limitation of this particular value for the contact angle is removed and an analytical solution of the potential flow problem inside an evaporating liquid line is presented, which is valid for any contact angle, θ_c, in the interval $(0, \pi/2)$. Following an appropriate adjustment in our analysis for $\theta_c > \pi/2$, a similar analytical solution is derived for strongly hydrophobic substrates, thus covering the entire domain of possible wettability conditions, $0 < \theta_c < \pi$. The stream function and velocity potential formulations are used to describe potential flow in the interior of the liquid and the Fourier transform is employed to derive an analytical solution, subject to boundary conditions that describe either pinned contact lines (decreasing contact angle) or depinned contact lines (constant contact angle). A general solution is derived, which is valid for any profile of the evaporation rate on the surface of the liquid. For illustration purposes, the results for kinetically-controlled evaporation are presented in terms of streamlines and equipotential lines, and, alternatively, in the form of the velocity vector field. A qualitative comparison with experimental results is attempted, aiming to elucidate the distinct behavior of suspended colloid matter during evaporation on hydrophilic and hydrophobic substrates. This work provides also information on the microflow inside evaporating liquid bodies on strongly hydrophobic substrates and, hopefully, will encourage further scientific activity in this area, both of theoretical and experimental nature.

II. MODEL DEVELOPMENT AND SOLUTION

Consider a liquid line shaped as a cylindrical segment lying on a flat surface (see Fig. 1). The coordinate system that describes naturally the boundaries of the physical problem is that of bicylinder coordinates α, β, z, which are related to the rectangular coordinates x, y, z through

$$x = c\frac{\sinh \alpha}{\cosh a + \cos \beta}, \tag{1a}$$

$$y = c\frac{\sin \beta}{\cosh a + \cos \beta}, \tag{1b}$$

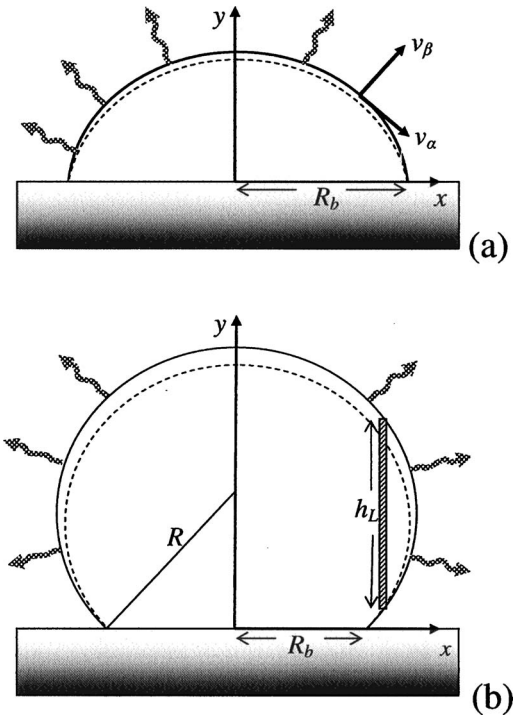

FIG. 1. Schematic representation of evaporating liquid line on (a) hydrophilic and (b) hydrophobic substrates.

$$z = z, \tag{1c}$$

where $-\infty < \alpha < +\infty$, $-\pi < \beta < \pi$, $-\infty < z < +\infty$, and $c = \text{constant} > 0$.

In numerous practical applications, including printing and substrate patterning, the length of the liquid line is much greater than the width of the wetted area. The liquid line can, then, be considered as infinitely long and the problem can be solved on a cross section only, using bipolar coordinates α, β (see Fig. 2). In this coordinate system, the curves given by

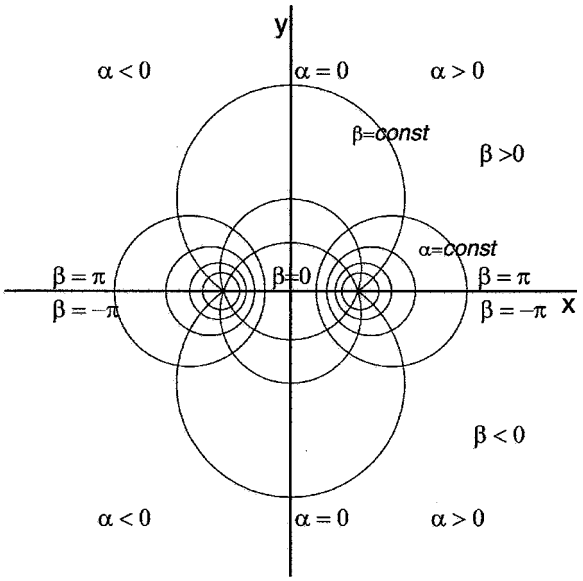

FIG. 2. Bipolar coordinate system.

β=constant are circular segments crossing the x axis at $x=\pm c$, whereas the curves given by α=constant are the corresponding orthogonal circles. The liquid line surface is the circular segment given by $\beta=\theta_c$, whereas the contact points are approached as $\alpha\rightarrow\pm\infty$. Note that parameter c of Eq. (1) coincides with R_b in Fig. 1, which is equal to half the width of the wetted area.

A. Potential flow formulation

Under the assumption of quasistatic flow, which is justified for relatively slow shape changes, the potential flow is described by

$$\Delta\varphi=0, \tag{2}$$

where φ is the velocity potential and relates to the velocity, v, by

$$v=\nabla\varphi. \tag{3}$$

In bipolar coordinates Eq. (2) takes the form

$$\left(\frac{\cosh\alpha+\cos\beta}{R_b}\right)^2\left(\frac{\partial^2\varphi}{\partial\alpha^2}+\frac{\partial^2\varphi}{\partial\beta^2}\right)=0 \tag{4}$$

and φ is connected to the α- and β-velocity components through the relations

$$v_\alpha=\frac{\cosh\alpha+\cos\beta}{R_b}\frac{\partial\varphi}{\partial\alpha}, \tag{5a}$$

$$v_\beta=\frac{\cosh\alpha+\cos\beta}{R_b}\frac{\partial\varphi}{\partial\beta}. \tag{5b}$$

The following boundary conditions apply for evaporation from the cylindrical surface:

$$\frac{\partial\varphi}{\partial\alpha}=0 \text{ at } \alpha=0, \tag{6a}$$

$$\frac{\partial\varphi}{\partial\alpha}=0 \text{ at } \alpha\rightarrow+\infty, \tag{6b}$$

$$\frac{\partial\varphi}{\partial\beta}=0 \text{ at } \beta=0, \tag{6c}$$

$$\frac{\partial\varphi}{\partial\beta}=\frac{R_b}{\cosh\alpha+\cos\beta}\left(u_{\mathrm{ns}}+\frac{J}{\rho}\right) \text{ at } \beta=\theta_c, \tag{6d}$$

where ρ is the liquid density, J is the local evaporation flux, and u_{ns} is the normal component of the surface velocity. The aforementioned boundary conditions express axial symmetry, Eq. (6a), finite velocity at the contact lines, Eq. (6b), impermeable solid surface, Eq. (6c), and the fact that the normal liquid velocity at the surface is the sum of the normal interface velocity and the mass transfer velocity, Eq. (6d).

The solution is obtained by application of the cosine Fourier transform to Eq. (4) followed by use of the boundary conditions (6a)–(6d). The final expression for the velocity potential is

$$\varphi(\alpha,\beta)=\frac{2R_b}{\pi}\int_0^\infty\frac{\cosh\lambda\beta\cos\lambda\alpha}{\lambda\sinh\lambda\theta_c}\times\left[\int_0^\infty\frac{(u_{\mathrm{ns}}+J/\rho)\cos\lambda a'}{\cosh a'+\cos\theta_c}da'\right]d\lambda. \tag{7}$$

The choice of the particular transform for real λ is dictated by the form of the boundary conditions, Eqs. (6). It can also been shown that the integrals in Eq. (7) remain finite for finite values of the evaporation flux, J.

The velocity components in bipolar coordinates can be calculated at every point inside the liquid line using Eqs. (5a), (5b), and (7),

$$v_\alpha(\alpha,\beta)=-\frac{2}{\pi}(\cosh\alpha+\cos\beta)\int_0^\infty\frac{\cosh\lambda\beta\sin\lambda\alpha}{\sinh\lambda\theta_c}\times\left[\int_0^\infty\frac{(u_{\mathrm{ns}}+J/\rho)\cos\lambda a'}{\cosh a'+\cos\theta_c}da'\right]d\lambda, \tag{8a}$$

$$v_\beta(\alpha,\beta)=\frac{2}{\pi}(\cosh\alpha+\cos\beta)\int_0^\infty\frac{\sinh\lambda\beta\cos\lambda\alpha}{\sinh\lambda\theta_c}\times\left[\int_0^\infty\frac{(u_{\mathrm{ns}}+J/\rho)\cos\lambda a'}{\cosh a'+\cos\theta_c}da'\right]d\lambda. \tag{8b}$$

In order to arrive at the x and y components of the velocity, an appropriate coordinate transformation is needed. The unit vector $\hat{\boldsymbol{e}}_i$ in the i direction is given by

$$\hat{\boldsymbol{e}}_i=\frac{1}{h_i}\frac{\partial\boldsymbol{r}}{\partial u_i}, \tag{9}$$

where $\boldsymbol{r}$ is the position vector, u_i is the corresponding coordinate, and h_i is the scale factor, given by

$$h_i=\left|\frac{\partial\boldsymbol{r}}{\partial u_i}\right|. \tag{10}$$

Combining Eqs. (1a)–(1c), (9), and (10) and following some algebraic manipulations, the relations between the unit vectors in bipolar and rectangular coordinates are obtained as follows:

$$\hat{\boldsymbol{e}}_\alpha=\frac{\cosh\alpha\cos\beta+1}{\cosh\alpha+\cos\beta}\hat{\boldsymbol{e}}_x-\frac{\sinh\alpha\sin\beta}{\cosh\alpha+\cos\beta}\hat{\boldsymbol{e}}_y, \tag{11a}$$

$$\hat{\boldsymbol{e}}_\beta=\frac{\sinh\alpha\sin\beta}{\cosh\alpha+\cos\beta}\hat{\boldsymbol{e}}_x+\frac{\cosh\alpha\cos\beta+1}{\cosh\alpha+\cos\beta}\hat{\boldsymbol{e}}_y. \tag{11b}$$

Finally, the velocity components in rectangular coordinates are given from

$$v_x(\alpha,\beta)=\frac{\cosh\alpha\cos\beta+1}{\cosh\alpha+\cos\beta}v_\alpha+\frac{\sinh\alpha\sin\beta}{\cosh\alpha+\cos\beta}v_\beta, \tag{12a}$$

$$v_y(\alpha,\beta)=-\frac{\sinh\alpha\sin\beta}{\cosh\alpha+\cos\beta}v_\alpha+\frac{\cosh\alpha\cos\beta+1}{\cosh\alpha+\cos\beta}v_\beta. \tag{12b}$$

B. Stream function formulation

An alternative approach is to use the stream function formulation, which will, in addition, provide direct information for the construction of the streamlines at any contact angle. Using the relation (see, for instance, [23])

$$\boldsymbol{v} = \left(\frac{1}{h_2 h_3} \frac{\partial \psi}{\partial u_2}, -\frac{1}{h_1 h_3} \frac{\partial \psi}{\partial u_1}, 0 \right) \tag{13}$$

one obtains for the bipolar coordinates of the velocity,

$$v_\alpha = \frac{\cosh \alpha + \cos \beta}{R_b} \frac{\partial \psi}{\partial \beta}, \tag{14a}$$

$$v_\beta = -\frac{\cosh \alpha + \cos \beta}{R_b} \frac{\partial \psi}{\partial \alpha}. \tag{14b}$$

For irrotational flow, $\nabla \times \boldsymbol{v} = 0$, which yields

$$\Delta \psi = 0. \tag{15}$$

The boundary conditions now become

$$\frac{\partial \psi}{\partial \beta} = 0 \text{ at } \alpha = 0, \tag{16a}$$

$$\frac{\partial \psi}{\partial \beta} = 0 \text{ at } \alpha \to +\infty, \tag{16b}$$

$$\frac{\partial \psi}{\partial \alpha} = 0 \text{ at } \beta = 0, \tag{16c}$$

$$\frac{\partial \psi}{\partial \alpha} = -\frac{R_b}{\cosh \alpha + \cos \beta} \left(u_{\mathrm{ns}} + \frac{J}{\rho} \right) \text{ at } \beta = \theta_c. \tag{16d}$$

The analytical solution of Eq. (15) subject to these boundary conditions is achieved with the help of the sine Fourier transform. The final expression is

$$\psi(\alpha, \beta) = -\frac{2R_b}{\pi} \int_0^\infty \frac{\sinh \lambda \beta \sin \lambda \alpha}{\lambda \sinh \lambda \theta_c} \times \left[\int_0^\infty \frac{(u_{\mathrm{ns}} + J/\rho) \cos \lambda a'}{\cosh a' + \cos \theta_c} da' \right] d\lambda, \tag{17}$$

which, of course, reproduces the same expressions for v_α and v_β as those obtained in the velocity potential formulation.

The expressions given in Eqs. (7), (8), and (17) involve the evaporation flux, J, and the normal velocity of the liquid at the interface, u_{ns}. The former relates directly to the controlling evaporation mechanism, namely, phase change, diffusion, or their combination, whereas the latter can be obtained as a function of the total evaporation rate from the liquid surface and the contact line condition. Below, the expressions that give u_{ns} as a function of the evaporation rate are given for hydrophilic ($0 < \theta_c < \pi/2$) and hydrophobic substrates ($\pi/2 < \theta_c < \pi$) in the cases of pinned and depinned contact lines. These expressions can then be introduced directly into the general expressions given in Eqs. (7), (8), and (17).

C. Hydrophilic substrates ($0 < \theta_c < \pi/2$)

1. Pinned contact lines

The volume of the liquid per unit length is given by

$$V_L = R_b^2 \frac{\theta_c - \cos \theta_c \sin \theta_c}{\sin^2 \theta_c}. \tag{18}$$

The total evaporation rate per unit length is

$$J_{\mathrm{TOT}} = 2 \frac{R_b}{\sin \theta_c} \int_{\pi/2 - \theta_c}^{\pi/2} J(\theta) d\theta, \tag{19}$$

where θ is the polar angle, the origin being located at the center of the underlying cylinder.

Under the pinned contact lines assumption, the wetting area remains constant, whereas the contact angle changes in a way that ensures cylindrical shape for the liquid line. In this case, the time derivative of the liquid volume is

$$\frac{dV_L}{dt} = 2R_b^2 \frac{\sin \theta_c - \theta_c \cos \theta_c}{\sin^3 \theta_c} \frac{d\theta_c}{dt}. \tag{20}$$

But

$$J_{\mathrm{TOT}} = -\rho \frac{dV_L}{dt}. \tag{21}$$

The combination of Eqs. (19)–(21) gives

$$\frac{d\theta_c}{dt} = -\frac{J_{\mathrm{TOT}}}{2\rho R_b^2} \frac{\sin^3 \theta_c}{\sin \theta_c - \theta_c \cos \theta_c}. \tag{22}$$

The height, h, at position x is given by

$$h = \sqrt{(R_b/\sin \theta_c)^2 - x^2} - R_b/\tan \theta_c. \tag{23}$$

From Eq. (23), following algebraic manipulations, one gets for constant R_b,

$$\left(\frac{\partial h}{\partial t} \right)_x = [1 - \cos \theta_c (1 - \bar{x}^2 \sin^2 \theta_c)^{-1/2}] \frac{R_b}{\sin^2 \theta_c} \frac{d\theta_c}{dt}. \tag{24}$$

and

$$\left(\frac{\partial h}{\partial x} \right)_t = -\bar{x} \sin \theta_c (1 - \bar{x}^2 \sin^2 \theta_c)^{-1/2}, \tag{25}$$

where $\bar{x} = x/R_b$.

The normal component of the surface velocity, u_{ns}, is given by

$$u_{\mathrm{ns}} = \frac{(\partial h/\partial t)_x}{\left[1 + \left(\frac{\partial h}{\partial x} \right)_t^2 \right]^{1/2}}. \tag{26}$$

Introduction of expressions (22), (24), and (25) into Eq. (26) gives

$$u_{\mathrm{ns}} = \frac{J_{\mathrm{TOT}}}{2\rho R_b} \frac{\sin \theta_c (\cos \theta_c - \sqrt{1 - \bar{x}^2 \sin^2 \theta_c})}{\sin \theta_c - \theta_c \cos \theta_c} \tag{27}$$

and in bipolar coordinates

$$u_{\mathrm{ns}} = -\frac{J_{\mathrm{TOT}}}{2\rho R_b}\frac{\sin^3\theta_c}{(\sin\theta_c - \theta_c\cos\theta_c)(\cosh\alpha + \cos\theta_c)}. \quad (28)$$

2. Depinned contact lines

In this case, the contact lines recede in a fashion that ensures constant contact angle and cylindrical shape for the liquid phase. The time derivative of the liquid volume is

$$\frac{dV_L}{dt} = 2R_b\frac{\theta_c - \sin\theta_c\cos\theta_c}{\sin^2\theta_c}\frac{dR_b}{dt}. \quad (29)$$

The combination of Eqs. (21) and (29) gives

$$\frac{dR_b}{dt} = -\frac{J_{\mathrm{TOT}}}{2\rho R_b}\frac{\sin^2\theta_c}{(\theta_c - \sin\theta_c\cos\theta_c)}. \quad (30)$$

From Eq. (23), following algebraic manipulations, one gets for constant θ_c,

$$\left(\frac{\partial h}{\partial t}\right)_x = [(1-\bar{x}^2\sin^2\theta_c)^{-1/2} - \cos\theta_c]\frac{1}{\sin\theta_c}\frac{dR_b}{dt}. \quad (31)$$

Introduction of expressions (25), (30), and (31) into Eq. (26) gives

$$u_{\mathrm{ns}} = \frac{J_{\mathrm{TOT}}}{2\rho R_b}\frac{\sin\theta_c(\cos\theta_c\sqrt{1-\bar{x}^2\sin^2\theta_c} - 1)}{\theta_c - \sin\theta_c\cos\theta_c} \quad (32)$$

and in bipolar coordinates

$$u_{\mathrm{ns}} = -\frac{J_{\mathrm{TOT}}}{2\rho R_b}\frac{\sin^3\theta_c\cosh\alpha}{(\theta_c - \sin\theta_c\cos\theta_c)(\cosh\alpha + \cos\theta_c)}. \quad (33)$$

D. Hydrophobic substrates ($\pi/2 < \theta_c < \pi$)

1. Pinned contact lines

For $\theta_c > \pi/2$, the height of the liquid surface measured from the solid surface, h, at any position x is given by

$$h = k\sqrt{(R_b/\sin\theta_c)^2 - x^2} - R_b/\tan\theta_c, \quad (34)$$

where $k=1$ for $0 \leqslant x \leqslant R$, R being is the radius of curvature of the liquid body, and $h \geqslant -R_b/\tan\theta_c$ and $k=-1$ for $R_b \leqslant x \leqslant R$ and $h \leqslant -R_b/\tan\theta_c$.

From Eq. (34), following algebraic manipulations, one gets for constant R_b,

$$\left(\frac{\partial h}{\partial t}\right)_x = [1 - k\cos\theta_c(1-\bar{x}^2\sin^2\theta_c)^{-1/2}]\frac{R_b}{\sin^2\theta_c}\frac{d\theta_c}{dt}. \quad (35)$$

The normal component of the surface velocity, u_{ns}, is in this case given by

$$u_{\mathrm{ns}} = k\frac{(\partial h/\partial t)_x}{\left[1 + \left(\frac{\partial h}{\partial x}\right)_t^2\right]^{1/2}}. \quad (36)$$

Introduction of expressions (22), (34), and (35) into Eq. (36) gives

$$u_{\mathrm{ns}} = \frac{J_{\mathrm{TOT}}}{2\rho R_b}\frac{\sin\theta_c(\cos\theta_c - k\sqrt{1-\bar{x}^2\sin^2\theta_c})}{\sin\theta_c - \theta_c\cos\theta_c}. \quad (37)$$

2. Depinned contact lines

From Eq. (34), following algebraic manipulations, one gets for constant θ_c,

$$\left(\frac{\partial h}{\partial t}\right)_x = [-\cos\theta_c + k(1-\bar{x}^2\sin^2\theta_c)^{-1/2}]\frac{1}{\sin\theta_c}\frac{dR_b}{dt}. \quad (38)$$

The combination of expressions (30), (34), (36), and (38) finally gives

$$u_{\mathrm{ns}} = \frac{J_{\mathrm{TOT}}}{2\rho R_b}\frac{\sin\theta_c(k\cos\theta_c\sqrt{1-\bar{x}^2\sin^2\theta_c} - 1)}{\theta_c - \sin\theta_c\cos\theta_c}. \quad (39)$$

E. Case study: Kinetically controlled evaporation

Once the profile of evaporation flux along the surface of the liquid body $J(\theta)$ is known, the solution provided here can offer the local flow field in the interior of the evaporating line. As a case study, the kinetically controlled mode is considered below, which is pertinent for slow phase change compared to vapor diffusion (e.g., nonvolatile solvents, low temperature evaporation, etc). In this case, the evaporation flux is constant across the surface of the liquid line, that is,

$$J(\theta) = \mathrm{const} = J_0. \quad (40)$$

In this case, Eq. (27) for hydrophilic substrates and pinned contact lines becomes

$$u_{\mathrm{ns}} = \frac{J_0}{\rho}\frac{\theta_c}{\sin\theta_c - \theta_c\cos\theta_c}(\cos\theta_c - \sqrt{1-\bar{x}^2\sin^2\theta_c}). \quad (41)$$

For hydrophobic substrates and pinned contact lines Eq. (37) becomes

$$u_{\mathrm{ns}} = \frac{J_0}{\rho}\frac{\theta_c}{\sin\theta_c - \theta_c\cos\theta_c}(\cos\theta_c - k\sqrt{1-\bar{x}^2\sin^2\theta_c}). \quad (42)$$

Substituting Eqs. (40) and (41) or (42) into Eqs. (7), (17), (8a), and (8b), the velocity potential, the stream function, and the local velocity can be determined for kinetically controlled evaporation of a cylindrical segment with pinned contact lines.

If the pinning assumption is removed and the contact lines are allowed to recede towards the center of the line, Eq. (32) gives for hydrophilic substrates

$$u_{\mathrm{ns}} = \frac{J_0}{\rho}\frac{\theta_c}{\theta_c - \sin\theta_c\cos\theta_c}(\cos\theta_c\sqrt{1-\bar{x}^2\sin^2\theta_c} - 1). \quad (43)$$

For hydrophobic substrates, Eq. (39) gives for depinned contact lines

$$u_{\mathrm{ns}} = \frac{J_0}{\rho}\frac{\theta_c}{\theta_c - \sin\theta_c\cos\theta_c}(k\cos\theta_c\sqrt{1-\bar{x}^2\sin^2\theta_c} - 1). \tag{44}$$

A straightforward dimensional analysis shows that, in all cases, the local velocity magnitude is directly proportional to the local evaporation flux, J_0. This is easily verified by insertion of Eqs. (41)–(44) into Eqs. (8a) and (8b).

F. Vertically-averaged liquid velocity

A quick measure of the inwards or outwards flow trend is provided by the vertically-averaged liquid velocity, which can be calculated from

$$\langle v_x\rangle = \frac{1}{h_L}\int_0^{h_L} v_x dy, \tag{45}$$

where h_L is the height of the vertical liquid column. Alternatively, one can calculate this velocity directly from the mass balance around a vertical liquid column of width δx and height h [10,11]. In the case of hydrophilic substrates $h_L = h$ and the mass balance reads [22]

$$\rho\left(\frac{\partial h_L}{\partial t}\right)_x = -\rho\left(\frac{\partial\langle v_x\rangle h_L}{\partial x}\right)_t - J\left[1+\left(\frac{\partial h_L}{\partial x}\right)^2\right]^{1/2}. \tag{46}$$

Introduction of Eqs. (24), (25), and (40) into Eq. (46) leads eventually to the vertically-averaged liquid velocity inside a kinetically controlled evaporating line with pinned contact lines lying on a hydrophilic substrate ($0 < \theta_c < \pi/2$),

$$\langle v_x\rangle = -\frac{R_b J_0}{\rho h_L(\sin\theta_c - \theta_c\cos\theta_c)}[\sin^{-1}(\bar{x}\sin\theta_c) - \theta_c\bar{x}]. \tag{47}$$

For depinned contact lines, the corresponding expression becomes

$$\langle v_x\rangle = \frac{R_b J_0\cos\theta_c}{\rho h_L(\theta_c - \sin\theta_c\cos\theta_c)}[\sin^{-1}(\bar{x}\sin\theta_c) - \theta_c\bar{x}]. \tag{48}$$

In the case of hydrophobic substrates ($\pi/2 < \theta_c < \pi$), Eq. (46) can be used only for $0 \leqslant x \leqslant R_b$. In the region that corresponds to $R_b \leqslant x \leqslant R$, the height of the liquid column becomes $h_L = 2\sqrt{(R_b/\sin\theta_c)^2 - x^2}$ [see Fig. 1(b)] and the mass balance becomes

$$\rho\left(\frac{\partial h_L}{\partial t}\right)_x = -\rho\left(\frac{\partial\langle v_x\rangle h_L}{\partial x}\right)_t - 2J\left[1+\frac{1}{2}\left(\frac{\partial h_L}{\partial x}\right)^2\right]^{1/2}. \tag{49}$$

The final expressions for the vertically averaged velocity in the region $0 \leqslant x \leqslant R_b$ are the same as those for hydrophilic substrates, namely, Eqs. (47) and (48) for pinned and depinned contact lines, respectively. However, for $R_b \leqslant x \leqslant R$ the corresponding expressions become

$$\langle v_x\rangle = -\frac{R_b J_0}{\rho h_L(\sin\theta_c - \theta_c\cos\theta_c)}[2\sin^{-1}(\bar{x}\sin\theta_c) - \pi], \tag{50}$$

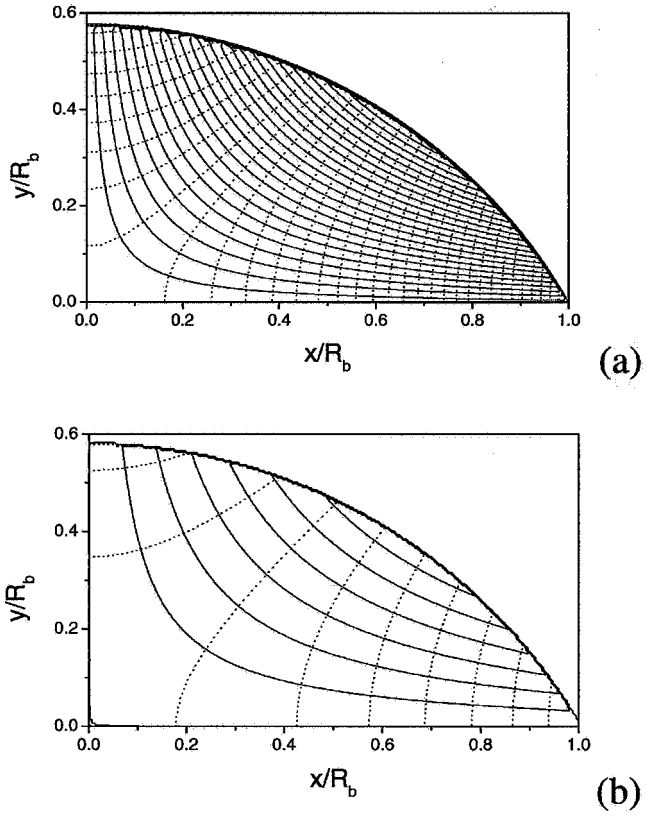

FIG. 3. Streamlines ($\delta\psi = 0.01$, solid lines) and equipotential lines ($\delta\varphi = 0.02$, dotted lines) inside an evaporating liquid line ($\theta_c = \pi/3$) with (a) pinned contact lines and (b) depinned contact lines.

$$\langle v_x\rangle = \frac{R_b J_0\cos\theta_c}{\rho h_L(\theta_c - \sin\theta_c\cos\theta_c)}[2\sin^{-1}(\bar{x}\sin\theta_c) - \pi], \tag{51}$$

for pinned and depinned contact lines, respectively.

III. RESULTS AND DISCUSSION

Numerical results for the internal flow field during evaporation with both pinned and depinned contact lines are presented in this section. For kinetically controlled evaporation, the streamlines and the equipotential lines for $\theta_c = \pi/3$ are shown in Figs. 3(a) and 3(b) for pinned and depinned contact lines, respectively. For the sake of comparison, equal stream function steps were used to draw the streamlines in the two figures. The same is true for the contours of the velocity potential in the two figures. The local flow field in terms of velocity vectors for $\theta_c = \pi/6$ is shown in Figs. 4(a) and 4(b), for pinned and depinned contact lines, respectively. The internal flow is directed from the center to the edges in the case of pinned contact lines, for any value of the contact angle $(0, \pi/2]$. This is held responsible for the promotion of a ring like deposit in the case of colloidal dispersions, commonly known as the coffee-stain phenomenon. On the contrary, for depinned contact lines, the liquid flow is directed towards the center of the liquid body favoring deposition of suspended particles away from the liquid edges.

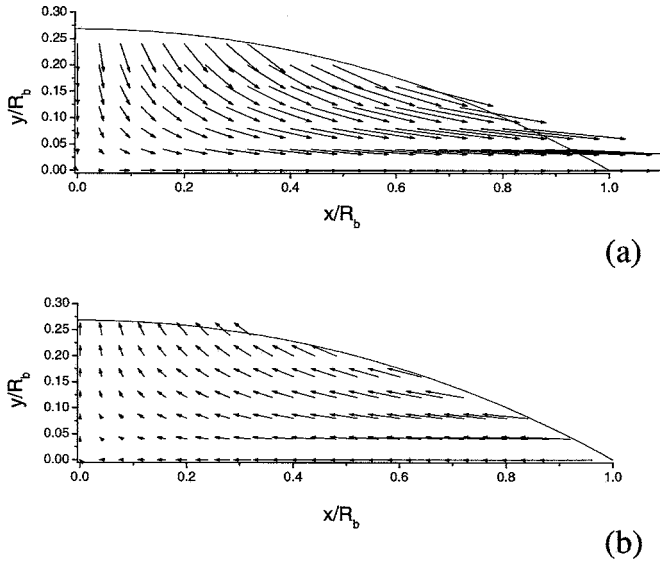

FIG. 4. Vector representation of the internal flow field in an evaporating line with contact angle $\theta_c=\pi/6$. (a) Pinned contact lines and (b) depinned contact lines.

In the case of contact angles greater than $\pi/2$ the internal flow is directed from the center to the edges for both pinned (see Fig. 5) and depinned contact lines. Although counterintuitive, the fact that flow is directed outwards even for depinned contact lines can be rationalized by geometric arguments, as shown in Fig. 6. Specifically, one may envisage an intermediate stage (dotted line) between initial (dashed line) and final (solid line) interface positions. This intermediate stage corresponds to the shape that the interface would assume if evaporation were to take place without any constraint regarding contact angle constancy. However, in order to keep the contact angle constant, the volume at this intermediate stage has to be redistributed, leading to the final interface shape. For hydrophobic substrates, it turns out that

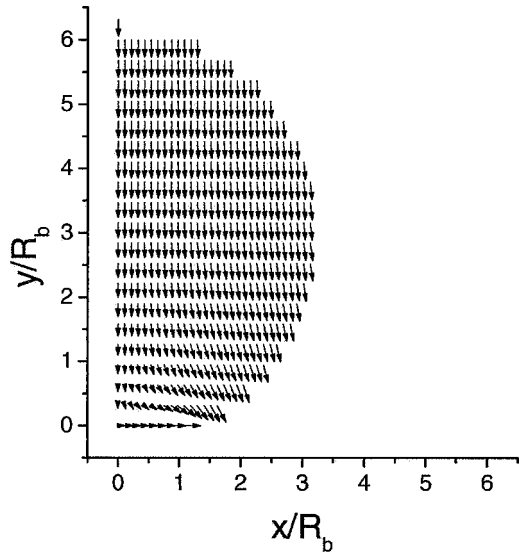

FIG. 5. Vector representation of the internal flow field in an evaporating line with pinned contact lines and contact angle $\theta_c=9\pi/10$.

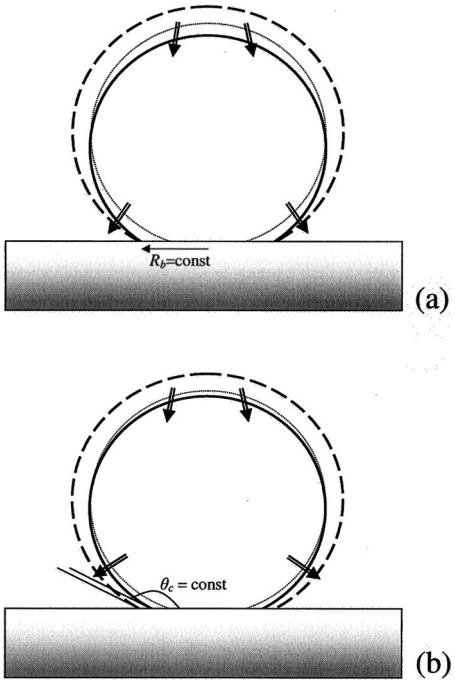

FIG. 6. Schematic representation of liquid boundaries during evaporation on a strongly hydrophobic substrate: (a) pinned contact lines and (b) depinned contact lines. Dashed lines: boundaries prior to the evaporation step. Dotted lines: hypothetical boundaries in the absence of any contact line constraint. Solid lines: boundaries after the evaporation step. Flow direction is from dotted to solid lines.

the final interface is placed lower than the one at the intermediate stage, extending also outwards, in accord with the analytical results for the local liquid velocity. The opposite behavior is observed in the depinned line case for hydrophilic substrates, corresponding to inward flow. However, it must be stressed that the velocity magnitude in the case of depinned contact lines is always smaller than that in the case of pinned contact lines at the same position and for the same values of evaporation rate and contact angle. This implies that more even deposition layers are to be expected for depinned contact lines than for pinned ones for the same set of operating conditions. The ratio of the local velocity inside a kinetically controlled evaporating line with depinned contact lines to that of pinned contact lines for any contact angle is shown in Fig. 7.

As expected, the flow field calculations as $\theta_c \to \pi/2$ given by Eqs. (8a) and (8b) coincide with those obtained using cylindrical coordinates in a previous work by the authors for the kinetic regime [22]. It is also noteworthy that in the particular case of $\theta_c=\pi/2$ and depinned contact lines, the velocity inside the liquid line becomes zero, since u_{ns} becomes equal to $-J_0/\rho$.

The normal component of the surface liquid velocity is found to change sign at position $x/R_b=\sqrt{\theta_c^2-\sin^2\theta_c}/(\theta_c \sin\theta_c)$, for both pinned and depinned contact lines in the case of hydrophilic substrates. In the case of pinned contact lines, the liquid flows outwards for x values larger than this critical value, whereas for smaller x values, the liquid flows inwards. The opposite phenomenon takes place in the depinned mode on hydrophilic substrates. For hydrophobic

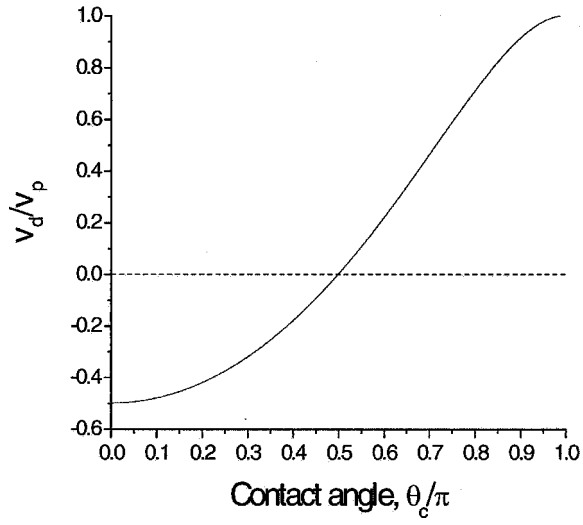

FIG. 7. Dependence of the ratio of velocity in an evaporating line with depinned contact lines to the velocity of an evaporating line with pinned contact lines vs contact angle.

substrates, the normal component of the liquid velocity at the surface changes from inwards to outwards at this critical value as x increases for both pinned and depinned contact lines.

Figures 8(a) and 8(b) show the variation of the vertically-averaged liquid velocity with the dimensionless distance from the center for different contact angles for pinned and depinned contact lines respectively. The use of Eq. (45) gives identical results as that of Eqs. (47), (48), (50), and (51), in each case, as expected. For hydrophilic substrates, the vertically-averaged liquid velocity magnitude increases almost linearly with x/R_b for small contact angle; as the contact angle increases, this linearity is confined to narrower regions around the center. It is also interesting to note that the vertically-averaged liquid velocity increases with increasing liquid wettability of the substrate for pinned lines. The same is true for depinned contact lines in hydrophilic substrates, whereas in hydrophobic substrates the magnitude of the vertically-averaged liquid velocity increases with decreasing liquid wettability up to a critical contact angle value $(\theta_c \approx \frac{11}{15}\pi)$ and starts decreasing for higher contact angle values.

A final observation on the vertically averaged liquid velocity concerns its magnitude for hydrophobic substrates as compared to that for hydrophilic ones. As hydrophobicity increases, much slower flows develop compared to that on strongly hydrophilic substrates, either inwards $(\theta_c < \pi/2)$ or outwards $(\theta_c > \pi/2)$. In both cases, the trend to coffee-stain development is limited; in fact, in the former case a crater-like deposit (i.e., increased accumulation in the central region) is expected due to the inward direction of liquid flow, in accord with experimental observations during evaporation of colloidal suspensions at large contact angles [16–18]. Further details on the expected deposition morphology can be extracted from the local flow field in the respective cases, as provided in the present work, especially if combined further with convective diffusion calculations.

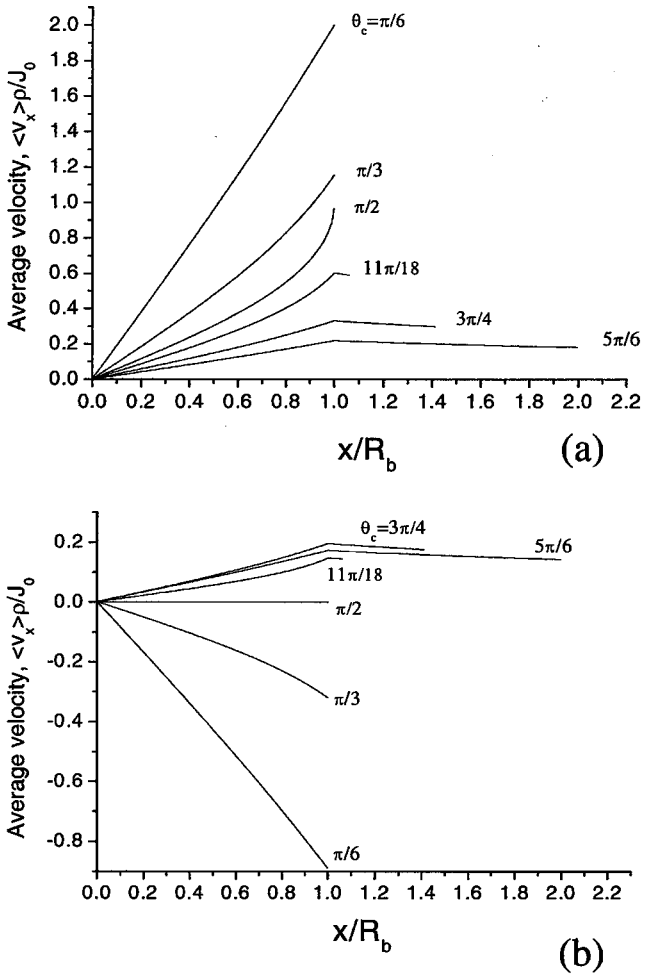

FIG. 8. Dimensionless vertically-averaged velocity vs. dimensionless radial distance on the substrate for various values of the contact angle: (a) pinned contact lines and (b) depinned contact lines.

IV. CONCLUDING REMARKS

An analytical solution to the problem of evaporation-induced potential flow inside a liquid line, shaped as a cylindrical segment lying on flat surface, is derived here. During evaporation, liquid mass is removed from the surface of the cylindrical line causing a shape change and giving rise to internal liquid flow aiming to restore the boundary requirements. It is assumed that the internal flow is sufficiently fast to justify quasistatic conditions despite the continuously changing shape of the liquid body. The solution derived here is valid for any mechanism of evaporation, for both pinned and depinned contact lines, provided that knowledge of the local evaporation flux is available. Although the potential flow model is probably not quite realistic for all practical cases, one can extract useful information on the flow field that develops and on the effects of the wettability, contact angle, and pinning condition on the flow trend during evaporation.

Flow field calculations in the kinetic evaporation regime reveal that the flow is always directed to the line edges if pinned, thus favoring the well-known coffee stain phenom-

enon, despite the fact that the local evaporation flux is uniform over the surface. On the contrary, inward liquid flow is observed for depinned contact lines for contact angles smaller than $\pi/2$ and uniform evaporation flux. The velocity magnitude increases with increasing wettability of the surface in both pinned and depinned cases.

The removal of the potential flow assumption is certainly a challenge in this line of work. Although similar qualitative conclusions are expected in the viscous flow case, an analytical expression for the local flow field in that case would provide useful input to deposition simulators, that could predict local deposition rates and, eventually, yield the corresponding deposition morphology for droplets made up of colloidal dispersions. This may be done, of course, using lubrication theory to obtain the flow field, followed by particle trajectory calculations, as in the case of evaporating DNA dispersions [9], but the validity of the solution would be confined to small contact angles only.

[1] H. Sirringhaus, T. Kawase, R. H. Friend, T. Shimoda, M. Inbasekaran, W. Wu, and E. P. Woo, Science **290**, 2123 (2000).
[2] T. Laurell, J. Nilsson, and G. Marko-Varga, Anal. Chem. **77**, 264A (2005).
[3] V. Dugas, J. Broutin, and E. Souteyrand, Langmuir **21**, 9130 (2005).
[4] T. Shimoda, K. Morii, S. Seki, and H. Kiguchi, MRS Bull. **28**, 821 (2003).
[5] T. Kawase, T. Shimoda, C. Newsome, H. Sirringhaus, and R. H. Friend, Thin Solid Films **438–439**, 279 (2003).
[6] K. Cheng, M.-H. Yang, W. W. W. Chiu, C.-Y. Huang, J. Chang, T.-F. Ying, and Y. Yang, Macromol. Rapid Commun. **26**, 247 (2005).
[7] E. Bonaccurso, H.-J. Butt, B. Hankeln, B. Niesenhaus, and K. Graf, Appl. Phys. Lett. **86**, 124101 (2005).
[8] A. Aksan, S. C. Morris, and M. Toner, Langmuir **21**, 2847 (2005).
[9] M. Chopra, L. Li, H. Hu, M. A. Burns, and R. G. Larson, J. Rheol. **47**, 1111 (2003).
[10] R. D. Deegan, O. Bakajin, T. F. Dupont, G. Huber, S. R. Nagel, and T. A. Witten, Phys. Rev. E **62**, 756 (2000).
[11] Y. O. Popov and T. A. Witten, Phys. Rev. E **68**, 036306 (2003).
[12] C. Bourgès-Monnier and M. E. R. Shanahan, Langmuir **11**, 2820 (1995).
[13] R. D. Deegan, O. Bakajin, T. F. Dupont, G. Huber, S. R. Nagel, and T. A. Witten, Nature (London) **389**, 827 (1997).
[14] M. Cachile, O. Bénichou, and A. M. Cazabat, Langmuir **18**, 7985 (2002).
[15] H. Hu and R. G. Larson, J. Phys. Chem. B **106**, 1334 (2002).
[16] K. Uno, K. Hayashi, T. Hayashi, K. Ito, and H. Kitano, Colloid Polym. Sci. **276**, 810 (1998).
[17] B.-J. de Gans and U. S. Schubert, Langmuir **20**, 7789 (2004).
[18] H.-Y. Ko, J. Park, H. Shin, and J. Moon, Chem. Mater. **16**, 4212 (2004).
[19] Y. Y. Tarasevich, Phys. Rev. E **71**, 027301 (2005).
[20] B. J. Fischer, Langmuir **18**, 60 (2002).
[21] H. Hu and R. G. Larson, Langmuir **21**, 3963 (2005).
[22] A. J. Petsi and V. N. Burganos, Phys. Rev. E **72**, 047301 (2005).
[23] L. G. Leal, *Laminar Flow and Convective Transport Processes: Scaling Principles and Asymptotic Analysis* (Butterworth-Heinemann, Boston, 1992).